A non-transgenic mouse model (icv-STZ mouse) of Alzheimer's disease: Similarities to and differences from the transgenic model (3xTg-AD mouse)

Yanxing Chen[1,2,*], **Zhihou Liang**[2,*], **Julie Blanchard**[1], **Chun-Ling Dai**[1], **Shenggang Sun**[2], **Moon H. Lee**[3], **Inge Grundke-Iqbal**[1], **Khalid Iqbal**[1], **Fei Liu**[1], and **Cheng-Xin Gong**[1]

[1]Department of Neurochemistry, New York State Institute for Basic Research in Developmental Disabilities, Staten Island, New York 10314, USA

[2]Department of Neurology, Union Hospital, Tongji Medical College, Huazhong University of Science & Technology, Wuhan, Hubei 430022, China

[3]Department of Developmental Neurobiology, New York State Institute for Basic Research in Developmental Disabilities, Staten Island, New York 10314, USA

Abstract

Alzheimer's disease (AD) can be divided into sporadic AD (SAD) and familial AD (FAD). Most AD cases are sporadic and result from multiple etiologic factors, including environmental, genetic and metabolic factors, whereas FAD is caused by mutations in the presenilins or amyloid-β (Aβ) precursor protein (APP) genes. A commonly used animal model for AD is the 3xTg-AD transgenic mouse model, which harbors mutated presenilin 1, APP and tau genes and thus represents a model of FAD. There is an unmet need to in the field to characterize animal models representing different AD mechanisms, so that potential drugs for SAD can be evaluated preclinically in these animal models. A mouse model generated by intracerebroventricular (icv) administration of streptozocin (STZ), the icv-STZ mouse, shows many aspects of SAD. In this study, we compared the non-cognitive and cognitive behaviors as well as biochemical and immunohistochemical alterations between the icv-STZ mouse and the 3xTg-AD mouse. We found that both mouse models showed increased exploratory activity as well as impaired learning and spatial memory. Both models also demonstrated neuroinflammation, altered synaptic proteins and insulin/IGF-1 (insulin-like growth factor-1) signaling, and increased hyperphosphorylated tau in the brain. The most prominent brain abnormality in the icv-STZ mouse was neuroinflammation, and in the 3xTg-AD mouse it was elevation of hyperphosphorylated tau. These observations demonstrate the behavioral and neuropathological similarities and differences between the icv-STZ mouse and the 3xTg-AD mouse models and will help guide future studies using these two mouse models for the development of AD drugs.

Keywords

Alzheimer's disease; mouse model; behavioral tests; brain pathology

---

Introduction

Alzheimer's disease (AD) is the leading cause of dementia and is characterized by progressive loss of memory and other cognitive functions. The neuropathological hallmarks of AD are extracellular senile plaques, consisting predominantly of the amyloid-β (Aβ), and neurofibrillary tangles (NFTs), consisting of hyperphosphorylated tau protein [1]. AD can be categorized into late-onset sporadic AD (SAD) and early-onset familial AD (FAD). FAD constitutes less than 1% of all AD cases [2], and most FAD is caused by mutations in the amyloid-β precursor protein (APP), presenilin-1 or presenilin-2 genes [3]. The vast majority of AD cases are SAD, which is multifactorial. SAD involves several etiopathogenic mechanisms. Neuroinflammation, head trauma, impaired brain glucose/energy metabolism, diabetes, and the presence of apoE ε4 allele are among the risk factors for AD [2].

A large number of animal models have been generated for investigation of AD mechanisms and evaluation of potential AD therapeutics in the last two decades. Most of these animal models are transgenic mouse models generated by over-expression of mutated human PS1, APP and/or tau. At present, a widely used AD model is the triple-transgenic 3xTg-AD mouse, which harbors three mutated transgenes (human $PS1_{M146V}$, APP_{Swe} and tau_{P301L}) and develops progressive, age-dependent amyloid plaques and NFTs, as well as memory deficits [4–9]. The transgenic mouse models are valuable tools to decipher the mechanisms of Alzheimer pathologies and some aspects of the disease mechanism. However, these models do not show all abnormalities seen in human AD and do not replicate the sporadic form of AD because SAD is not caused by any known mutations or overexpression of APP. Thus, there is an unmet need in the field to characterize animal models representing different AD mechanisms, so that potential drugs can be evaluated preclinically in these animal models of various AD mechanisms.

A rodent model that shows many aspects of SAD abnormalities had been generated by intracerebroventricular (icv) injection of streptozotocin (STZ) [10,11]. STZ is a diabetogenic compound and is commonly used to induce diabetes in animals when administered in the periphery due to its activity to damage the pancreatic β cells and to induce insulin resistance [12]. A well established brain abnormality of SAD is a decrease in brain glucose/energy metabolism, which correlates to the severity of dementia symptoms in AD [13,14]. Brain insulin signaling regulates cerebral glucose metabolism [15], and impaired brain insulin signaling transduction has been reported in AD [16–18]. Brain insulin resistance, decreased brain glucose metabolism, cholinergic deficits, accumulation of tau and Aβ, oxidative stress, gliosis and learning and memory deficits have been reported in the icv-STZ mice and rats [19,20].

In this study, we investigated the behavioral, biochemical and pathological abnormalities of the icv-STZ mouse and compare them with those seen in the 3xTg-AD mouse. The comparison of these two commonly used AD mouse models will guide the selection of mouse models for future AD research.

Materials and Methods

Antibodies and Reagents

Primary antibodies used in this study are listed in Table 1. Peroxidase-conjugated anti-mouse and anti-rabbit IgG were obtained from Jackson ImmunoResearch Laboratories (West Grove, PA, USA). The enhanced chemiluminescence (ECL) kit was from Pierce (Rockford, IL, USA). ABC staining system was from Santa Cruz Biotechnology (CA, USA). Other chemicals were from Sigma (St. Louis, MO, USA).

Animals

The 3xTg-AD homozygous mice harboring $PS1_{M146V}$, APP_{Swe} and tau_{P301L} transgenes and the genetic background–matched wild type (WT) control mice (a hybrid 129/Sv and C57BL/6 mice) were initially obtained from F.M. LaFerla through the Jackson Laboratory (New Harbor, 124 ME, USA). Mice were housed and bred in accordance with the approved protocol from our Institutional Animal Care and Use Committee, according to the PHS Policy on Human Care and Use of Laboratory animals (revised March 15, 2010). Mice were housed (4~5 animals per cage) with a 12/12 h light/dark cycle and with ad libitum access to food and water.

The icv-STZ mice were produced by stereotaxic injection of STZ [2–deoxy–2–(3–(methyl–3–nitrosoureido)-D-glucopyranose), from Sigma-Aldrich (St. Louis, MO)] into the left lateral ventricle of 6 months old, female the WT mice. Briefly, mice were first anesthetized using 2.5% avertin (2,2,2 tribromoethanol, Sigma-Aldrich) and then restrained onto a stereotaxic apparatus. The bregma coordinates used for injection were: −1.0 mm lateral, −0.3 mm posterior and −2.5 mm below. Each mouse received a single icv injection of 3.0 mg/kg STZ in 3.0 μl 0.9% saline into the left ventricle of the brain. The control WT mice and the 3xTg-AD mice (all female, 6 months old) also received icv injection of 3.0 μl 0.9% saline. Twenty one days after icv injection, the mice were subjected to a battery of behavioral tests which lasted for 3 weeks (Fig. 1a). Finally, the mice were sacrificed by decapitation, and the brains were removed immediately. The hippocampus, cerebral cortex, peri-ventricle area, cerebellum and brain stem were dissected, flash frozen in dry ice, and stored in −80°C for biochemical analyses. Some brains were fixed with 4% paraformaldehyde in 0.1 M PBS, followed by cryoprotection in 30% sucrose. Sagittal sections (40-μm thick) were cut on a freezing microtome. The sections were stored in glycol anti-freeze solution (ethylene glycol, glycerol, and 0.1 M PBS in 3:3:4 ratio) at −20°C until immunohistochemical staining.

In this study, we included 18 3xTg-AD mice, 26 icv-STZ mice and 18 WT control mice for all behavioral tests, and 7–9 mice per group for biochemical and immunohistochemical analyses.

Elevated plus maze

Elevated plus maze was used to evaluate anxiety/emotionality of the mice. It consisted of four arms (30 × 5 cm) connected by a common 5 × 5 cm center area. Two opposite facing arms were open (OA), whereas the other two facing arms were enclosed by 20 cm high walls (CA). The entire plus-maze was elevated on a pedestal to a height of 82 cm above floor level in a room separated from the investigator. The mouse was placed onto the central area facing an open arm and allowed to explore the maze for a single 8 min session. Between each session, any feces were cleared from the maze, and the maze floor was cleaned with 70% alcohol to remove any urine or scent cues. The number of CA entries, OA entries, and the amount of time spent in CA and OA were automatically recorded by a video tracking system (ANY-Maze version 4.5 software, Stoelting Co., Wood Dale, IL, USA).

Open field

Anxiety and exploratory activities were evaluated by allowing mice to freely explore an open field arena for 15 min. The testing apparatus was a classic open field (i.e. a PVC square arena, 50 × 50 cm, with walls 40 cm high), surmounted by a video camera connecting to a computer. Each mouse was placed individually at the arena and the performance was monitored and the time spent in the center and peripheral area and the distance traveled in the arena were automatically recorded by a video tracking system (ANY-Maze version 4.5 software, Stoelting Co.).

One-trial object recognition task

Mice were tested for one-trial object recognition based on the innate tendency of rodents to differentially explore novel objects over familiar ones in an open field arena, using a procedure modified from a previously described one [21]. The procedure consisted of three different phases: a habituation phase, a sample phase, and a test phase. Following initial exposure, four additional 10 min daily habituation sessions were introduced for mice to become familiar with the apparatus and the surrounding environment. On the fifth day, every mouse was first submitted to the sample phase for which two identical objects were placed in a symmetric position from the center of the arena and was allowed to freely explore the objects for 5 min. After a 15-min delay during which the mouse was returned to its home cage, the animal was reintroduced in the arena to perform the test phase. The mouse was then exposed to two objects for another 5 min: a familiar object (previously presented during the sample phase) and a novel object, placed at the same location as during the sample phase. Data collection was performed using a video tracking system (ANY-Maze version 4.5 software, Stoelting Co.). Object discrimination was evaluated by the index: [(time spent exploring the new object)/(time spent exploring both old and new objects)] during the test phase.

Accelerating Rotarod test

Motor coordination and balance of mice were assessed by using a Rotarod test. Tests on accelerating Rotarod was conducted by giving each mouse two sessions of three trials on a rotating cylinder. The speed increased steadily from 4 to 40 rpm over a 5-min period. The latency to fall off the Rotarod was calculated. Inter-trial intervals were 10–15 min for each mouse.

Morris water maze

Spatial reference learning and memory were evaluated in a water maze adapted from that previously described by Morris and collaborators [22]. The test was performed in a white pool of 180 cm in diameter filled with water tinted with non-toxic white paint and maintained at room temperature ($21 \pm 2°C$). During training, a platform (14 cm in diameter) was submerged 1 cm below water surface. All mice were given 4 trials per day for four consecutive days. The starting position was randomized among four quadrants of the pool. For each trial, the animal was given 90 sec to locate the hidden platform. If a mouse failed to find the platform within 90 sec, it was gently guided to it. At the end of each trial, the mouse was left on the platform for 20 sec, then dried and returned to its home cage until the next trial. Probe trial was given 24 h after the last day of training. During the probe trial, mice were allowed to swim in the pool for 60 sec, but without the escape platform. The latency to reach the platform (sec), swim distance (cm), and swim speed (cm/sec) were recorded using an automated tracking system (Smart video tracking system, Panlab, Harvard Apparatus).

Western Blot Analysis

The hippocampi were homogenized in pre-chilled buffer containing 50 mM tris-HCl (pH7.4), 50 mM GlcNAc, 20 μM UDP, 2.0 mM EGTA, 2 mM Na_3VO_4, 50 mM NaF, 20 mM β-glycerophosphate, 0.5 mM AEBSF, 10 μg/ml aprotinin, 10 μg/ml leupeptin, and 4 μg/ml pepstatin A. Protein concentrations of the homogenates were determined by using modified Lowery method [23]. The Samples were resolved in 10% or 12.5% SDS-PAGE and electrotransferred onto Immobilon-P membrane (Millipore, Bedford, MA). The blots were then probed with primary antibody and developed with the corresponding horseradish peroxidase–conjugated secondary antibody and enhanced chemiluminescence kit (Pierce, Rockford, IL). Densitometric quantification of protein bands in Western blots were analyzed by using the TINA software (Raytest IsotopenmeBgerate GmbH, Straubenhardt, Germany).

Immunohistochemical staining

Floating sections were incubated for 30 min with 0.3% H_2O_2 and 0.3% Triton X-100 for 15 min at room temperature, washed in PBS and blocked in a solution containing 5% normal goat serum and 0.1% Triton X-100 for 30 min. Sections were then incubated overnight at 4°C with primary antibody before applying biotinylated secondary antibody and then avidin/ biotinylated horseradish peroxidase (Santa Cruz Biotechnology). The sections were stained with peroxidase substrate and then mounted on microscope slides (Brain Research Laboratories, Newton, MA, USA), dehydrated, and covered with coverslips.

Statistical analysis

All data were analyzed with GraphPad software using ANOVA, followed by Tukey's post hoc test. Data are presented as mean ± SEM. $p < 0.05$ or lower was considered to be significant.

Results

General behavior characterization

To eliminate the effects of icv injection itself, the control mice and the 3xTg-AD mice were also subjected to the injection procedure, but with saline only. We monitored general conditions and body weight changes after icv injection. We found that the mouse body weight of all three groups declined in the first week after icv injection procedure. The body weight of the saline-injected mice (Control and 3xTg-AD mice), but not the STZ-injected mice (icv-STZ mice), recovered afterwards (Fig. 1b). Adult 3xTg-AD mice had smaller body weights than the WT controls, which is consistent with previous reports on these mice [24].

We found that the icv-STZ mice had the same Rotarod performance as control mice, indicating no impairment of motor coordination or balance for the icv-STZ mice (Fig. 1c). As we observed previously [24], the 3xTg-AD mice showed much better performance on Rotarod. We also measured the spontaneous locomotor and exploratory activity of the mice in an open field test. Both icv-STZ and 3xTg-AD mice showed increased horizontal activity (total distance traveled in the arena) (Fig. 1d), suggesting increased exploratory activity. These mice also spent less time on the open arms in an elevated plus maze (Fig. 1e). The elevated plus maze is the most widely used test to measure the anxiety-like behavior in rodents [25].

Cognitive impairment of icv-STZ mice and 3xTg-AD mice

To examine the short-term memory, we conducted one-trial object recognition task with a 15-min interval between the sample phase and the test phase. As compared to the control mice, both the icv-STZ mice and the 3xTg-AD mice spent less time exploring the novel object than the familiar object, although all mice spent similar time for exploring during the sample phase (Fig. 2a). Accordingly, the discrimination indexes of icv-STZ mice and 3xTg-AD mice were significantly lower than the control mice (Fig. 2b). These results clearly indicated a short-term memory impairment in the icv-STZ mice and the 3xTg-AD mice.

We employed Morris water maze to investigate the spatial reference learning and memory of these mice. There were no statistical differences among groups in swim speed, suggesting that the velocity is similar in all groups (Fig. 2c). During the training phase, all mice learnt the platform location, as revealed by a decrease in the latency (data not shown) and the distance traveled (Fig. 2d) to locate the submerged platform. However, the training was delayed for the icv-STZ mice and the 3xTg-AD mice as they needed more time (data not shown) and traveled a longer distance to find the platform than the control mice (Fig. 2d).

These results suggest an impairment to encode and remember the spatial coordinates of the platform within the environment. Retrieval of spatial memory was more specifically analyzed with the probe trials performed 24 hours after the last training trial. Memory performance was determined by the number of the former platform site crossings and the percentage of time/distance animals spent/traveled in the target quadrant. As compared to the control mice, the icv-STZ mice and the 3xTg-AD mice crossed the former platform site much less often than control mice (Fig. 2e) and did not show marked preference toward the target quadrant (Fig. 2f). These results indicate that the icv-STZ mice and the 3xTg-AD mice have decreased ability to encode the environment as a spatial map and to localize the platform, suggesting an impairment of spatial reference memory.

More marked neuroinflammation in brains of icv-STZ mice than of 3xTg-AD mice

Neuroinflammation, as reflected by astrogliosis and microglial activation, has been well established in AD brain [26]. To investigate neuroinflammation, we determined the levels of GFAP, a marker of astrocytes, and Iba1, a marker of microglia, in the hippocampus of the icv-STZ and 3xTg-AD mice by Western blots. We found marked increase in the levels of both GFAP and Iba1 in both mouse models, as compared to control mice (Fig. 3a, 3b). Higher elevation was seen in the icv-STZ mice than the 3xTg-AD mice.

To confirm the glial activation and its topographic distribution in the icv-STZ and 3xTg-AD mice, we stained frozen brain sections with antibodies to these two glial markers. We found a marked increase in GFAP-positive astrocytes throughout the brains of the icv-STZ mice (Fig. 3c). Strongest staining was seen in the hippocampus and the periventricle area. Increased GFAP staining was also seen in the 3xTg-AD mice, but the increase was not as marked as in the icv-STZ mice and was restricted mainly in the hippocampus and the periventricle area. Similar to astrocytes, marked increase in microglias, as stained with anti-Iba1, was also observed throughout the brains of the icv-STZ mice (Fig. 3c). Such an increase was also seen in the 3xTg-AD mice, but the increase was not as marked as in the icv-STZ mice. These studies revealed more glial activation in the icv-STZ mice than the 3xTg-AD mice and suggest more severe neuroinflammation in the hippocampus than other areas of the brain in these two mouse models.

Alterations of synaptic proteins in icv-STZ mice and 3xTg-AD mice

Synapses are structural basis of memory, which depends on synaptic plasticity that is in turn regulated by modulation of neurotransmitter release at the pre-synaptic site and of the number, types or properties of neurotransmitter receptors at the post-synaptic site. Therefore, we studied the levels of pre- and post-synaptic proteins in these two mouse models. We observed a marked decrease of synaptophysin, a pre-synaptic marker, in the hippocampus of icv-STZ mice, but not of 3xTg-AD mice, by Western blots (Fig. 4a, b). The level of the postsynaptic marker, postsynaptic density 95 (PSD95), was not changed in either model. We also determined the levels of AMPA receptor (GluR1 and GluR2/3) and NMDA receptor (NR1). We found decreased AMPA receptor GluR2/3 in the hippocampus of both models, but the decrease reached statistical significance only in the icv-STZ mice. GluR1 also tended to be decreased in the icv-STZ mice. No significant changes in the level of NR1 were observed in either mouse models. These results demonstrate differential abnormalities of synaptic plasticity in these two mouse models.

The reduction of synaptophysin in the hippocampus of icv-STZ mice and of GluR2/3 in the hippocampus of both mouse models was confirmed by immunohistochemical studies. The reduced immunostaining was seen in all sectors of the hippocampus (Fig. 4c). In addition, reduced immunostaining of synaptophysin in icv-STZ mice and of GluR2/3 in both models was also seen in the cerebral cortex.

Dysregulation of brain insulin/IGF-1 signaling in icv-STZ mice and 3xTg-AD mice

Brain insulin/insulin-like growth factor-1 (IGF-1) signaling has gained increasing interest in the AD field because its impairment appears to be involved in SAD [27]. We thus compared the levels and the activation of each component of the signaling pathway, including IR, IGF-1R, IRS1, PI3K, PDK1, AKT and GSK. The activation status of these components was assessed by measuring the phosphorylation level of these proteins because their activities are dependent on phosphorylation at the specific sites we detected. We observed alterations of both the levels and the phosphorylation/activation of several components of the insulin/IGF-1 signaling pathway in the hippocampus of both icv-STZ mice and 3xTg-AD mice (Fig. 5). In the icv-STZ mice, both the level and the phosphorylation of IRS1 and the regulatory subunit of PI3K (PI3K p85) were found to be upregulated, whereas the phosphorylation/activation of PDK1 was downregulated, as compared to control mice (Fig. 5a, b).

The dysregulation of the insulin/IGF-1 signaling appeared to be more remarkable in the 3xTg-AD mice than in the icv-STZ mice. In the 3xTg-AD mouse hippocampus, upregulation of several upstream components (IRS1, IRS1 pS307, PI3K p85 and P-PI3K p85) and downregulation of several downstream components (PDK1, PKD1 pS241, AKT, AKT pS473, GSK3α/β and phosphorylated GSK3α/β) of the insulin/IGF-1 signaling pathway were observed. These results revealed bidirectional dysregulation of the insulin/IGF-1 signaling, suggesting aberrant crosstalk with other brain signaling transduction pathways in the brains of these two mouse models.

When the phosphorylation of each component of the insulin/IGF-1 signaling pathway was calculated after being normalized with the level of the corresponding protein, we found significant decrease in PDK1 phosphorylation in the icv-STZ mice and increase in phosphorylation of AKT and GSK3α in the 3xTg-AD mice (Fig. 5c).

Phosphorylation of tau in icv-STZ mice and 3xTg-AD mice

Tau protein is abnormally hyperphosphorylated and accumulated in AD brain, which appears to underlie neurodegeneration. Thus, we also investigated level and total tau and phosphorylated tau in the brains of icv-STZ mice and 3xTg-AD mice. As expected, we observed that the level of tau protein in the hippocampus of 3xTg-AD mice was approximately 4-fold higher than that of control mice due to over-expression of human tau in the transgenic mouse brains (Fig. 6a, c). There was no change in tau level in the brains of icv-STZ mice. We studied several AD-relevant tau phosphorylation sites and found an increase in tau that was phosphorylated at Ser199/202 and Thr205, but a decrease in tau that was phosphorylated at Ser214, in the hippocampus of icv-STZ mice (Fig. 6a, c). The increase in tau phosphorylated at Ser199/202 and Thr205 represented a net increase in tau phosphorylation because the increase was still seen after normalizing with the total tau level (Fig. 6b). In the 3xTg-AD mouse hippocampus, a marked increase in tau phosphorylated at all the phosphorylation sites studied was observed, as compared to controls (Fig. 6c). This increase in hyperphosphorylated tau at this age (7.5-month old) appears to result from the marked increase (4-fold) in the total tau in 3xTg-AD mice (Fig. 6c), because after normalization of the phosphorylated tau levels with the level of total tau (as detected by antibody R134d), no significant increase in tau phosphorylation at any of the sites studied was seen (data not shown).

Discussion

The major clinical phenotype of AD patients is the progressive decline in cognition. Therefore, any valid AD animal model should show cognitive impairment. In accordance with previous studies [28,29], we observed an impairment of short-term memory using

object recognition task and reference spatial memory in Morris water maze for both icv-STZ mice and 3xTg-AD mice. The icv-STZ mice were indistinguishable from the 3xTg-AD mice in these impairments at the age of 7 months studied. Cognitive impairment is known to exacerbate in an age-dependent manner in 3xTg-AD mice [29]. Long-term retention deficits in 3xTg-AD mice start to manifest at the age of 4–5 months, and short-term memory is affected by the age of 6–7 months. When these mice are 18-month old, they are unable to learn the platform location in the water maze, indicating inability to encode and/or remember spatial information, a characteristic of cognitive failure relative to hippocampal impairment. Longitudinal studies of behavioral assessments for icv-STZ mice are lacking. However, memory deficits have been reported in icv-STZ rodents from 24 hours to 3 months after STZ injection [11,30,10,31].

Behavioral and psychological symptoms of AD, also known as neuropsychiatric symptoms, include symptoms like agitation, aberrant motor behavior, anxiety, depression and hallucinations. It is estimated that neuropsychiatric symptoms affect up to 90% of all dementia patients which dramatically affect the quality of life of both AD patients and their caregivers [32]. The non-cognitive behavioral changes, therefore, need to be investigated for characterization of AD animal models. Abnormalities in non-cognitive behaviors have been implicated in various transgenic mice including the 3xTg-AD mice [33]. Icv-STZ mice have also been shown to exhibit increased anxiety-like behavior in the elevated plus maze [34]. In the present study, we observed increased exploratory activity in the open field and avoidance of the open arms in the elevated plus maze of both the icv-STZ and the 3xTg-AD mice, indicating increased restless and anxious-like behavior. These observations suggest that both icv-STZ and 3xTg-AD mice model some aspects of the neuropsychiatric symptoms of AD and the icv-STZ mice exibit more marked behavioral abnormalities than the 3xTg-AD mice.

Neuroinflammtion, as reflected by astrogliosis and microglial activation, is another prominent feature that is thought to contribute to AD pathogenesis [35]. It has been reported to correlate directly with the cognitive decline in AD patients [36]. In agreement with previous reports [28,37–41,9,42], we observed astrogliosis and microglial activation in both icv-STZ and 3xTg-AD mice. The neuroinflamation was much more remarkable and widespread in the brains of icv-STZ mice than the 3xTg-AD mice. The precise trigger of inflammation in AD brain remains controversial. In the 3xTg-AD mice, microglia is activated in a progressive and age-dependent manner and appears to correspond to the emergence of early intracellular Aβ and hyperphosphorylated tau pathology [42]. Activation of astrocytes are readily visible in 3xTg-AD mice brains at the age of 2 months, but do not show noticeable age-related enhancement of GFAP-positive astrocytes staining [9]. In icv-STZ mouse brains, the pronounced neuroinflammation is likely caused by neuronal damage from STZ-induced oxidative stress [38]. It is known that STZ upon decomposition gives rise to H_2O_2 and NO [43], and NO formation after STZ icv injection is independent of NO synthase activity [37]. Oxidative stress in the icv-STZ rodents has been widely reported by several groups [38,44–50]. Treatment with antioxidants can alleviate STZ-induced cognitive impairment and restore biochemical changes in the brain [44–50].

Synaptic dysfunction and loss occur in the initial stages of AD, correlate better with cognitive deficits than plaques and tangles, and are believed to be the structural basis of cognitive impairment [51–53]. In the present study, we found marked reduction in synaptophysin and GluR2/3 in the brains of icv-STZ mice, suggesting synaptic damage in these mice. The AMPA receptor subunits GluR2/3 also tended to be decreased in 3xTg-AD mice, but it did not reach statistical significance. However, impaired basal synaptic transmission and LTP have been reported in 6-month old 3xTg-AD mice [4]. The impaired memory of the 3xTg-AD mice at this age might attribute to the loss of functional synapses

or subtle changes in both the magnitude and distribution of effective synaptic coupling without causing substantial synapse loss [54]. The discrepancy between synaptic proteins and electrophysiological results has been reported before in aged rats [55].

With the observation of abnormalities in glucose/energy metabolism and insulin signaling in AD brain, the "insulin-resistant brain state" has been hypothesized to play a central role in neurodegeneration in SAD. The icv-STZ rodent model is suggested to be a suitable model for SAD with regards to insulin-resistant brain state [20]. In the present study, we observed alterations in the levels and phosphorylation/activation of several components of the insulin/IGF-1 signaling pathway, but we did not find a uniform downregulation of this signaling pathway. Our observations are consistent with previous studies that show normal level and phosphorylation state of IR, but elevated the tyrosine kinase activity in the hippocampus of icv-STZ rats [10]. We found more remarkable dysregulation of the insulin/IGF-1 signaling pathway in the hippocampus of the 3xTg-AD mice than the icv-STZ mice. In the 3xTg-AD mice, we found upregulation of several upstream components (IRS1, IRS1 pS307, PI3K p85 and P-PI3K p85) and downregulation of several downstream components (PDK1, PKD1 pS241, AKT, AKT pS473, GSK3α/β and phosphorylated GSK3α/β) of the insulin/IGF-1 signaling pathway. The upregulation of the upstream components of the insulin/IGF-1 signaling pathway seen in the 3xTg-AD mouse brains might have resulted from compensatory responses to the decreased downstream components. The relative increase in phosphorylation of AKT and GSK3α seen in the 3xTg-AD mice might also result from a negative feedback of the marked decrease in their protein levels. Alternatively, if there is aberrant crosstalk of the insulin/IGF-1 signaling pathway with other brain signaling transduction pathways, it might have led to the downregulation of the downstream components despite upregulation of the upstream components of the insulin/IGF-1 signaling pathway.

We also investigated phosphorylation of tau in the hippocampus of both models. We observed an increase in tau phosphorylation at Ser199/202 and Thr205, but not at several other phosphorylation sites studied. Increased tau phosphorylation at Thr212 and Ser396 has also been reported in icv-STZ rats [10,56]. It is not surprising to see a dramatic increase in total tau and phosphorylated tau level in the hippocampus of the 3xTg-AD mice because of overexpression of mutated human tau_{P301L}. Marked increase in tau phosphorylated at all the sites we studied appears to result merely from tau overexpression, because the total tau level was similarly increased in the 3xTg-AD mice. To our knowledge, the present study is the first to compare, by using Western blots, phosphorylated tau in the hippocampus between the 3xTg-AD mice and the WT control mice at such a young age. Oddo et al. investigated the formation of NFTs by immunohistochemistry, but they did not observe any tangles at the age of 6 months [4,5]. A more detailed immunohistochemical study on the progression of brain pathology in 3xTg-AD mice found significant accumulation of phosphorylated tau in the hippocampus and amygdala, starting at the age of 6 months [9], which is consistent to our biochemical analyses. Though tau phosphorylation manifested at the age of 7 months in the current study, gallyas positive neurons and sarkosyl insoluble tau aggregates are known to become first detectable at the age of 12 months in this mouse model [4,5,9,57]. Since little Aβ is detectable in the brains of the icv-STZ mice within 3 months after STZ injection [58], we did not investigate Aβ in this study.

In summary, we compared for the first time behavioral and brain abnormalities between the icv-STZ mice, a model of SAD, and 3xTg-AD mice, a commonly used model of FAD. Our studies indicate that although these two mouse models show similar behavioral deficits, they demonstrated different brain abnormalities. Despite alterations of both mouse models in several aspects, the most obvious brain alteration of the icv-STZ mice was neuroinflammation, whereas accumulation of hyperphosphorylated tau and Aβ [4,5,9] were

prominent in the 3xTg-AD mice. Therefore, these two animal models can serve as models of different mechanisms and aspects of AD for future studies of disease mechanisms and preclinical drug discovery.

Acknowledgments

References

1. Grundke-Iqbal I, Iqbal K, Tung YC, Quinlan M, Wisniewski HM, Binder LI. Abnormal phosphorylation of the microtubule-associated protein tau (tau) in Alzheimer cytoskeletal pathology. Proc Natl Acad Sci U S A. 1986; 83 (13):4913–4917. [PubMed: 3088567]

2. Iqbal K, Grundke-Iqbal I. Alzheimer's disease, a multifactorial disorder seeking multitherapies. Alzheimers Dement. 2010; 6(5):420–424.10.1016/j.jalz.2010.04.006 [PubMed: 20813343]

3. Waring SC, Rosenberg RN. Genome-wide association studies in Alzheimer disease. Arch Neurol. 2008; 65(3):329–334.10.1001/archneur.65.3.329 [PubMed: 18332245]

4. Oddo S, Caccamo A, Shepherd JD, Murphy MP, Golde TE, Kayed R, Metherate R, Mattson MP, Akbari Y, LaFerla FM. Triple-transgenic model of Alzheimer's disease with plaques and tangles: intracellular Abeta and synaptic dysfunction. Neuron. 2003; 39 (3):409–421. [PubMed: 12895417]

5. Oddo S, Caccamo A, Kitazawa M, Tseng BP, LaFerla FM. Amyloid deposition precedes tangle formation in a triple transgenic model of Alzheimer's disease. Neurobiol Aging. 2003; 24 (8):1063–1070. [PubMed: 14643377]

6. Janelsins MC, Mastrangelo MA, Oddo S, LaFerla FM, Federoff HJ, Bowers WJ. Early correlation of microglial activation with enhanced tumor necrosis factor-alpha and monocyte chemoattractant protein-1 expression specifically within the entorhinal cortex of triple transgenic Alzheimer's disease mice. J Neuroinflammation. 2005; 2:23.10.1186/1742-2094-2-23 [PubMed: 16232318]

7. Billings LM, Oddo S, Green KN, McGaugh JL, LaFerla FM. Intraneuronal Abeta causes the onset of early Alzheimer's disease-related cognitive deficits in transgenic mice. Neuron. 2005; 45(5):675–688.10.1016/j.neuron.2005.01.040 [PubMed: 15748844]

8. Clinton LK, Billings LM, Green KN, Caccamo A, Ngo J, Oddo S, McGaugh JL, LaFerla FM. Age-dependent sexual dimorphism in cognition and stress response in the 3xTg-AD mice. Neurobiol Dis. 2007; 28(1):76–82.10.1016/j.nbd.2007.06.013 [PubMed: 17659878]

9. Mastrangelo MA, Bowers WJ. Detailed immunohistochemical characterization of temporal and spatial progression of Alzheimer's disease-related pathologies in male triple-transgenic mice. BMC Neurosci. 2008; 9:81.10.1186/1471-2202-9-81 [PubMed: 18700006]

10. Grunblatt E, Salkovic-Petrisic M, Osmanovic J, Riederer P, Hoyer S. Brain insulin system dysfunction in streptozotocin intracerebroventricularly treated rats generates hyperphosphorylated tau protein. J Neurochem. 2007; 101(3):757–770.10.1111/j.1471-4159.2006.04368.x [PubMed: 17448147]

11. Salkovic-Petrisic M, Tribl F, Schmidt M, Hoyer S, Riederer P. Alzheimer-like changes in protein kinase B and glycogen synthase kinase-3 in rat frontal cortex and hippocampus after damage to the insulin signalling pathway. J Neurochem. 2006; 96(4):1005–1015.10.1111/j.1471-4159.2005.03637.x [PubMed: 16412093]

12. Szkudelski T. The mechanism of alloxan and streptozotocin action in B cells of the rat pancreas. Physiol Res. 2001; 50 (6):537–546. [PubMed: 11829314]

13. Drzezga A, Lautenschlager N, Siebner H, Riemenschneider M, Willoch F, Minoshima S, Schwaiger M, Kurz A. Cerebral metabolic changes accompanying conversion of mild cognitive impairment into Alzheimer's disease: a PET follow-up study. Eur J Nucl Med Mol Imaging. 2003; 30(8):1104–1113.10.1007/s00259-003-1194-1 [PubMed: 12764551]

14. Heiss WD, Szelies B, Kessler J, Herholz K. Abnormalities of energy metabolism in Alzheimer's disease studied with PET. Ann N Y Acad Sci. 1991; 640:65–71. [PubMed: 1776760]

15. Duarte AI, Moreira PI, Oliveira CR. Insulin in central nervous system: more than just a peripheral hormone. J Aging Res. 2012:384017.10.1155/2012/384017 [PubMed: 22500228]

16. Liu Y, Liu F, Grundke-Iqbal I, Iqbal K, Gong CX. Deficient brain insulin signalling pathway in Alzheimer's disease and diabetes. J Pathol. 2011; 225(1):54–62.10.1002/path.2912 [PubMed: 21598254]

17. Steen E, Terry BM, Rivera EJ, Cannon JL, Neely TR, Tavares R, Xu XJ, Wands JR, de la Monte SM. Impaired insulin and insulin-like growth factor expression and signaling mechanisms in Alzheimer's disease--is this type 3 diabetes? J Alzheimers Dis. 2005; 7 (1):63–80. [PubMed: 15750215]

18. Talbot K, Wang HY, Kazi H, Han LY, Bakshi KP, Stucky A, Fuino RL, Kawaguchi KR, Samoyedny AJ, Wilson RS, Arvanitakis Z, Schneider JA, Wolf BA, Bennett DA, Trojanowski JQ, Arnold SE. Demonstrated brain insulin resistance in Alzheimer's disease patients is associated with IGF-1 resistance, IRS-1 dysregulation, and cognitive decline. J Clin Invest. 2012; 122(4): 1316–1338.10.1172/jci59903 [PubMed: 22476197]

19. Salkovic-Petrisic M, Hoyer S. Central insulin resistance as a trigger for sporadic Alzheimer-like pathology: an experimental approach. J Neural Transm Suppl. 2007; (72):217–233. [PubMed: 17982898]

20. Salkovic-Petrisic M, Osmanovic J, Grunblatt E, Riederer P, Hoyer S. Modeling sporadic Alzheimer's disease: the insulin resistant brain state generates multiple long-term morphobiological abnormalities including hyperphosphorylated tau protein and amyloid-beta. J Alzheimers Dis. 2009; 18(4):729–750.10.3233/jad-2009-1184 [PubMed: 19661616]

21. Sargolini F, Roullet P, Oliverio A, Mele A. Effects of intra-accumbens focal administrations of glutamate antagonists on object recognition memory in mice. Behav Brain Res. 2003; 138 (2): 153–163. [PubMed: 12527446]

22. Morris RG, Garrud P, Rawlins JN, O'Keefe J. Place navigation impaired in rats with hippocampal lesions. Nature. 1982; 297 (5868):681–683. [PubMed: 7088155]

23. Bensadoun A, Weinstein D. Assay of proteins in the presence of interfering materials. Anal Biochem. 1976; 70 (1):241–250. [PubMed: 1259145]

24. Blanchard J, Wanka L, Tung YC, del Cardenas-Aguayo MC, LaFerla FM, Iqbal K, Grundke-Iqbal I. Pharmacologic reversal of neurogenic and neuroplastic abnormalities and cognitive impairments without affecting Abeta and tau pathologies in 3xTg-AD mice. Acta Neuropathol. 2010; 120 (5): 605–621. [PubMed: 20697724]

25. Pellow S, Chopin P, File SE, Briley M. Validation of open:closed arm entries in an elevated plus-maze as a measure of anxiety in the rat. J Neurosci Methods. 1985; 14 (3):149–167. [PubMed: 2864480]

26. Wyss-Coray T, Rogers J. Inflammation in Alzheimer disease-a brief review of the basic science and clinical literature. Cold Spring Harb Perspect Med. 2012; 2(1):a006346.10.1101/cshperspect.a006346 [PubMed: 22315714]

27. Correia SC, Santos RX, Perry G, Zhu X, Moreira PI, Smith MA. Insulin-resistant brain state: the culprit in sporadic Alzheimer's disease? Ageing Res Rev. 2011; 10(2):264–273.10.1016/j.arr. 2011.01.001 [PubMed: 21262392]

28. Prickaerts J, Fahrig T, Blokland A. Cognitive performance and biochemical markers in septum, hippocampus and striatum of rats after an i.c.v. injection of streptozotocin: a correlation analysis. Behav Brain Res. 1999; 102 (1–2):73–88. [PubMed: 10403017]

29. Gimenez-Llort L, Blazquez G, Canete T, Johansson B, Oddo S, Tobena A, LaFerla FM, Fernandez-Teruel A. Modeling behavioral and neuronal symptoms of Alzheimer's disease in mice: a role for intraneuronal amyloid. Neurosci Biobehav Rev. 2007; 31(1):125–147.10.1016/j.neubiorev.2006.07.007 [PubMed: 17055579]

30. Dou J, Cui C, Dufour F, Alkon DL, Zhao WQ. Gene expression of alpha-endosulfine in the rat brain: correlative changes with aging, learning and stress. J Neurochem. 2003; 87 (5):1086–1100. [PubMed: 14622089]

31. Mayer G, Nitsch R, Hoyer S. Effects of changes in peripheral and cerebral glucose metabolism on locomotor activity, learning and memory in adult male rats. Brain Res. 1990; 532 (1–2):95–100. [PubMed: 2149302]

32. Cerejeira J, Lagarto L, Mukaetova-Ladinska EB. Behavioral and psychological symptoms of dementia. Front Neurol. 2012; 3:73.10.3389/fneur.2012.00073 [PubMed: 22586419]

33. Sterniczuk R, Antle MC, Laferla FM, Dyck RH. Characterization of the 3xTg-AD mouse model of Alzheimer's disease: part 2. Behavioral and cognitive changes. Brain Res. 2010; 1348:149–155.10.1016/j.brainres.2010.06.011 [PubMed: 20558146]

34. Pinton S, da Rocha JT, Gai BM, Nogueira CW. Sporadic dementia of Alzheimer's type induced by streptozotocin promotes anxiogenic behavior in mice. Behav Brain Res. 2011; 223(1):1–6.10.1016/j.bbr.2011.04.014 [PubMed: 21515307]

35. McGeer EG, McGeer PL. Inflammatory processes in Alzheimer's disease. Prog Neuropsychopharmacol Biol Psychiatry. 2003; 27(5):741–749.10.1016/s0278-5846(03)00124-6 [PubMed: 12921904]

36. Simpson JE, Ince PG, Lace G, Forster G, Shaw PJ, Matthews F, Savva G, Brayne C, Wharton SB. Astrocyte phenotype in relation to Alzheimer-type pathology in the ageing brain. Neurobiol Aging. 2010; 31(4):578–590.10.1016/j.neurobiolaging.2008.05.015 [PubMed: 18586353]

37. Prickaerts J, De Vente J, Honig W, Steinbusch H, Ittersum MMV, Blokland A, Steinbusch HW. Nitric oxide synthase does not mediate neurotoxicity after an i.c.v. injection of streptozotocin in the rat. J Neural Transm. 2000; 107 (7):745–766. [PubMed: 11005541]

38. Weinstock M, Shoham S. Rat models of dementia based on reductions in regional glucose metabolism, cerebral blood flow and cytochrome oxidase activity. J Neural Transm. 2004; 111(3):347–366.10.1007/s00702-003-0058-y [PubMed: 14991459]

39. Rodrigues L, Biasibetti R, Swarowsky A, Leite MC, Quincozes-Santos A, Quilfeldt JA, Achaval M, Goncalves CA. Hippocampal alterations in rats submitted to streptozotocin-induced dementia model are prevented by aminoguanidine. J Alzheimers Dis. 2009; 17(1):193–202.10.3233/jad-2009-1034 [PubMed: 19494442]

40. Shoham S, Bejar C, Kovalev E, Schorer-Apelbaum D, Weinstock M. Ladostigil prevents gliosis, oxidative-nitrative stress and memory deficits induced by intracerebroventricular injection of streptozotocin in rats. Neuropharmacology. 2007; 52(3):836–843.10.1016/j.neuropharm. 2006.10.005 [PubMed: 17123555]

41. Lester-Coll N, Rivera EJ, Soscia SJ, Doiron K, Wands JR, de la Monte SM. Intracerebral streptozotocin model of type 3 diabetes: relevance to sporadic Alzheimer's disease. J Alzheimers Dis. 2006; 9 (1):13–33. [PubMed: 16627931]

42. Kitazawa M, Oddo S, Yamasaki TR, Green KN, LaFerla FM. Lipopolysaccharide-induced inflammation exacerbates tau pathology by a cyclin-dependent kinase 5-mediated pathway in a transgenic model of Alzheimer's disease. J Neurosci. 2005; 25(39):8843–8853.10.1523/jneurosci. 2868-05.2005 [PubMed: 16192374]

43. Takasu N, Komiya I, Asawa T, Nagasawa Y, Yamada T. Streptozocin- and alloxan-induced H2O2 generation and DNA fragmentation in pancreatic islets. H2O2 as mediator for DNA fragmentation. Diabetes. 1991; 40 (9):1141–1145. [PubMed: 1834504]

44. Javed H, Khan MM, Ahmad A, Vaibhav K, Ahmad ME, Khan A, Ashafaq M, Islam F, Siddiqui MS, Safhi MM. Rutin prevents cognitive impairments by ameliorating oxidative stress and neuroinflammation in rat model of sporadic dementia of Alzheimer type. Neuroscience. 2012; 210:340–352.10.1016/j.neuroscience.2012.02.046 [PubMed: 22441036]

45. Isik AT, Celik T, Ulusoy G, Ongoru O, Elibol B, Doruk H, Bozoglu E, Kayir H, Mas MR, Akman S. Curcumin ameliorates impaired insulin/IGF signalling and memory deficit in a streptozotocin-treated rat model. Age (Dordr). 2009; 31(1):39–49.10.1007/s11357-008-9078-8 [PubMed: 19234767]

46. Saxena G, Patro IK, Nath C. ICV STZ induced impairment in memory and neuronal mitochondrial function: A protective role of nicotinic receptor. Behav Brain Res. 2011; 224(1):50–57.10.1016/j.bbr.2011.04.039 [PubMed: 21620901]

47. Javed H, Khan MM, Khan A, Vaibhav K, Ahmad A, Khuwaja G, Ahmed ME, Raza SS, Ashafaq M, Tabassum R, Siddiqui MS, El-Agnaf OM, Safhi MM, Islam F. S-allyl cysteine attenuates

oxidative stress associated cognitive impairment and neurodegeneration in mouse model of streptozotocin-induced experimental dementia of Alzheimer's type. Brain Res. 2011; 1389:133–142.10.1016/j.brainres.2011.02.072 [PubMed: 21376020]

48. Ishrat T, Parveen K, Khan MM, Khuwaja G, Khan MB, Yousuf S, Ahmad A, Shrivastav P, Islam F. Selenium prevents cognitive decline and oxidative damage in rat model of streptozotocin-induced experimental dementia of Alzheimer's type. Brain Res. 2009; 1281:117–127.10.1016/j.brainres.2009.04.010 [PubMed: 19374888]

49. Ishrat T, Hoda MN, Khan MB, Yousuf S, Ahmad M, Khan MM, Ahmad A, Islam F. Amelioration of cognitive deficits and neurodegeneration by curcumin in rat model of sporadic dementia of Alzheimer's type (SDAT). Eur Neuropsychopharmacol. 2009; 19(9):636–647.10.1016/j.euroneuro.2009.02.002 [PubMed: 19329286]

50. Dhull DK, Jindal A, Dhull RK, Aggarwal S, Bhateja D, Padi SS. Neuroprotective effect of cyclooxygenase inhibitors in ICV-STZ induced sporadic alzheimer's disease in rats. J Mol Neurosci. 2012; 46(1):223–235.10.1007/s12031-011-9583-6 [PubMed: 21701788]

51. Arendt T. Synaptic degeneration in Alzheimer's disease. Acta Neuropathol. 2009; 118(1):167–179.10.1007/s00401-009-0536-x [PubMed: 19390859]

52. Terry RD, Masliah E, Salmon DP, Butters N, DeTeresa R, Hill R, Hansen LA, Katzman R. Physical basis of cognitive alterations in Alzheimer's disease: synapse loss is the major correlate of cognitive impairment. Ann Neurol. 1991; 30(4):572–580.10.1002/ana.410300410 [PubMed: 1789684]

53. Selkoe DJ. Alzheimer's disease is a synaptic failure. Science. 2002; 298(5594):789–791.10.1126/science.1074069 [PubMed: 12399581]

54. Barnes CA. Do synaptic markers provide a window on synaptic effectiveness in the aged hippocampus? Neurobiol Aging. 1999; 20(3):349–351. discussion 359–360. [PubMed: 10588584]

55. Nicolle MM, Gallagher M, McKinney M. No loss of synaptic proteins in the hippocampus of aged, behaviorally impaired rats. Neurobiol Aging. 1999; 20 (3):343–348. [PubMed: 10588583]

56. Deng Y, Li B, Liu Y, Iqbal K, Grundke-Iqbal I, Gong CX. Dysregulation of insulin signaling, glucose transporters, O-GlcNAcylation, and phosphorylation of tau and neurofilaments in the brain: Implication for Alzheimer's disease. Am J Pathol. 2009; 175(5):2089–2098.10.2353/ajpath.2009.090157 [PubMed: 19815707]

57. Oddo S, Caccamo A, Cheng D, Jouleh B, Torp R, LaFerla FM. Genetically augmenting tau levels does not modulate the onset or progression of Abeta pathology in transgenic mice. J Neurochem. 2007; 102(4):1053–1063.10.1111/j.1471-4159.2007.04607.x [PubMed: 17472708]

58. Salkovic-Petrisic M, Osmanovic-Barilar J, Bruckner MK, Hoyer S, Arendt T, Riederer P. Cerebral amyloid angiopathy in streptozotocin rat model of sporadic Alzheimer's disease: a long-term follow up study. J Neural Transm. 2011; 118(5):765–772.10.1007/s00702-011-0651-4 [PubMed: 21533606]

59. Tatebayashi Y, Iqbal K, Grundke-Iqbal I. Dynamic regulation of expression and phosphorylation of tau by fibroblast growth factor-2 in neural progenitor cells from adult rat hippocampus. J Neurosci. 1999; 19 (13):5245–5254. [PubMed: 10377336]

60. Pei JJ, Gong CX, Iqbal K, Grundke-Iqbal I, Wu QL, Winblad B, Cowburn RF. Subcellular distribution of protein phosphatases and abnormally phosphorylated tau in the temporal cortex from Alzheimer's disease and control brains. J Neural Transm. 1998; 105 (1):69–83. [PubMed: 9588762]
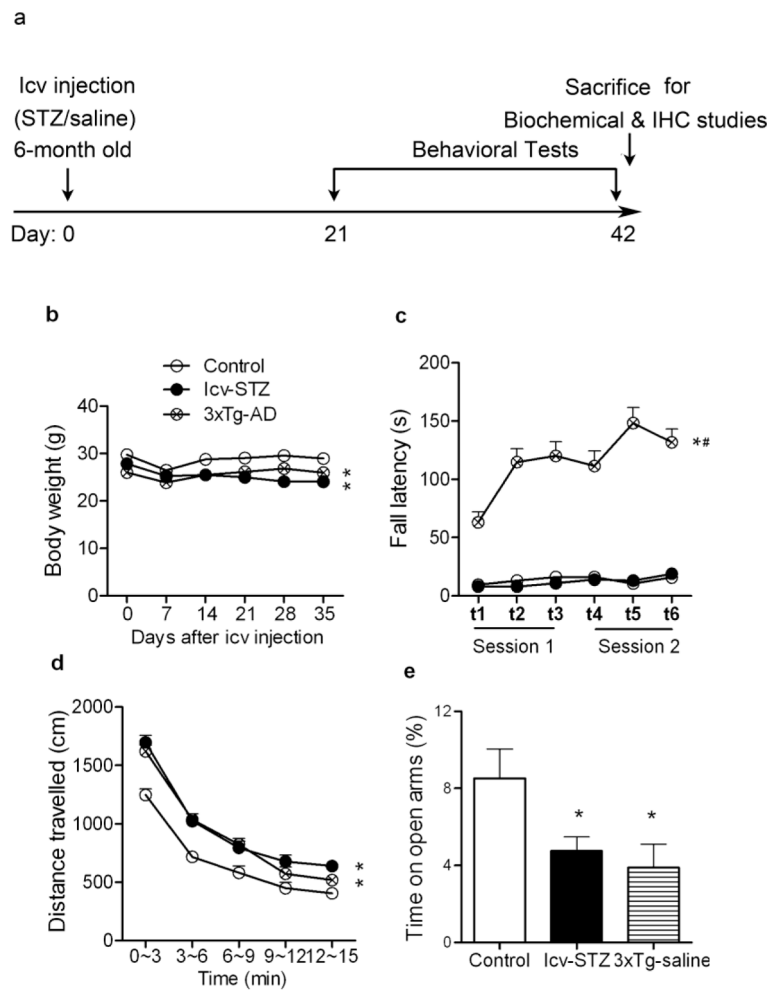
Fig. 1.
Animal study design (a) and general behavioral characterization (b–f). The body weight of mice after icv injection was monitored once a week (b). Motor coordination and balance were evaluated using accelerating rotarod (c). Spontaneous locomotor and exploratory activity was assessed in an open field (d). Anxiety-like behaviors were evaluated in an elevated plus maze, and the time spent in the open arms over the total time spent in the maze (open plus close arms) is shown (e). Data are reported as mean ± SEM. *, $p < 0.05$ vs. control mice. [#], $p < 0.05$ vs. icv-STZ mice
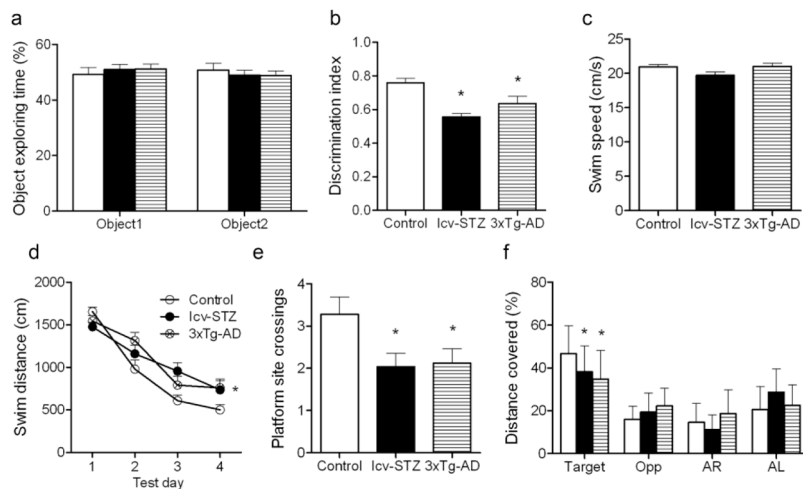
Fig. 2.
Behavioral tests of mice using one-trial object recognition task and Morris water maze. One-trial object recognition task was carried out in an open field. Time spent exploring two identical objects during sample phase are shown as percentage of object exploring time (a). Object discrimination during test phase is presented by the discrimination index (time exploring the novel object/total time for exploring) (b). Spatial memory of the mice was tested in the Morris water maze (c–f). The average swim speed in the whole tests (c), the distances traveled to the hidden platform during training (d), the number of the platform site crossings during the probe trial (e), and the percentage of distance traveled in the target, opposite (Opp), adjacent right (AR) and adjacent left (AL) quandrants during probe trial (f) are shown. Data are reported as mean ± SEM. *, $p < 0.05$ vs. control mice
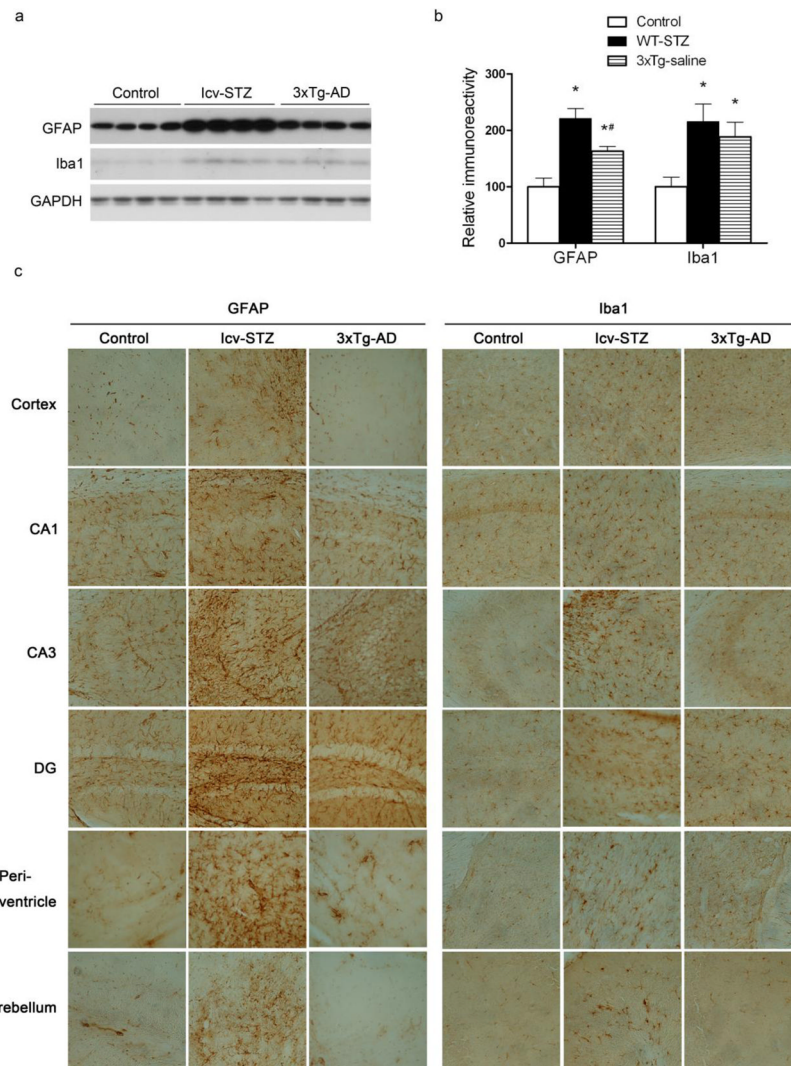
Fig. 3.
Neuroinflammation markers in the brains of icv-STZ mice and 3xTg-AD mice. (a) Hippocampi from control, icv-STZ and 3xTg-AD mice were analyzed by Western blots developed with antibodies against GFAP, Iba1 and, as a loading control, GAPDH. (b) Densitometric quantifications (mean ± SEM) of the blots after being normalized with the GAPDH levels. *, $p < 0.05$ vs. control mice. #, $p < 0.05$ vs. icv-STZ mice. (c) Representative DAB staining images of frozen brain sections of the mice (magnification: 20x)
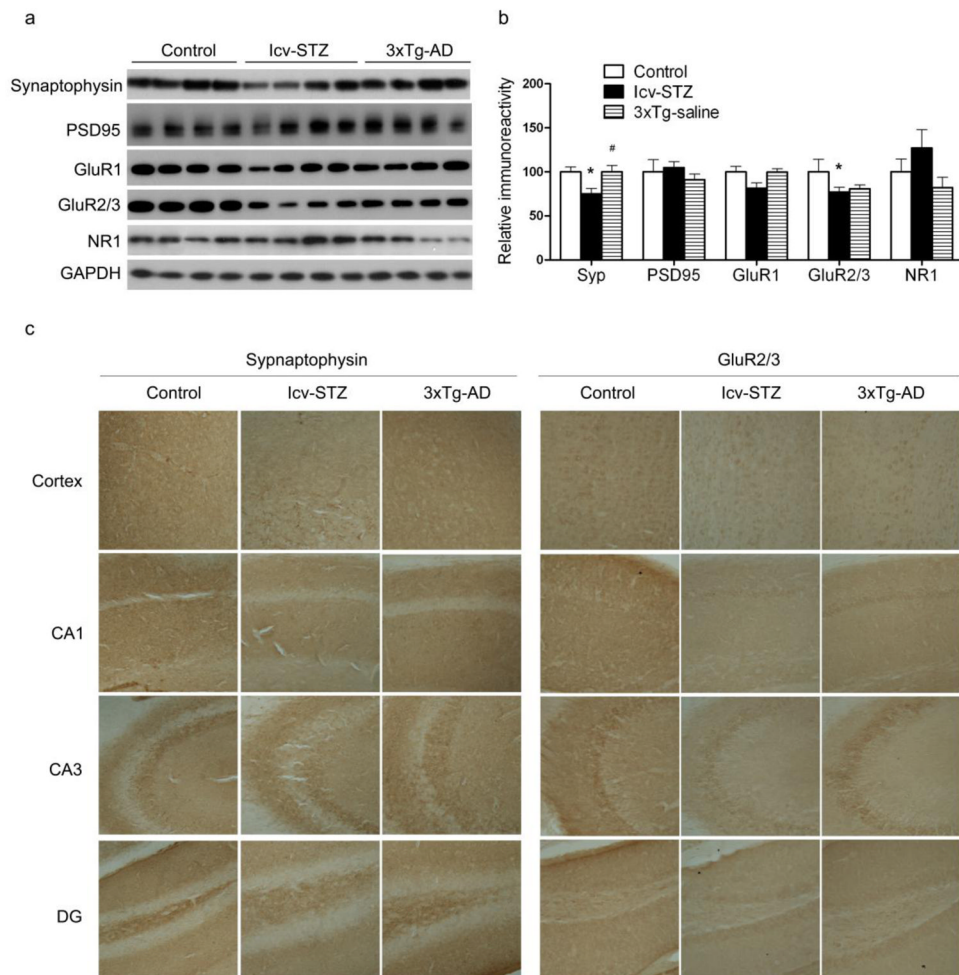
Fig. 4.
Synaptic proteins in icv-STZ mice and 3xTg-AD mice. (a) Hippocampi from control, icv-STZ and 3xTg-AD mice were analyzed by Western blots developed with antibodies indicated on the left of the blots. (b) Densitometric quantifications (mean ± SEM) of the blots after being normalized with the GAPDH levels. *, $p < 0.05$ vs. control mice. [#], $p < 0.05$ vs. icv-STZ mice. (c) Representative DAB staining images of frozen brain sections of the mice (magnification: 20x)
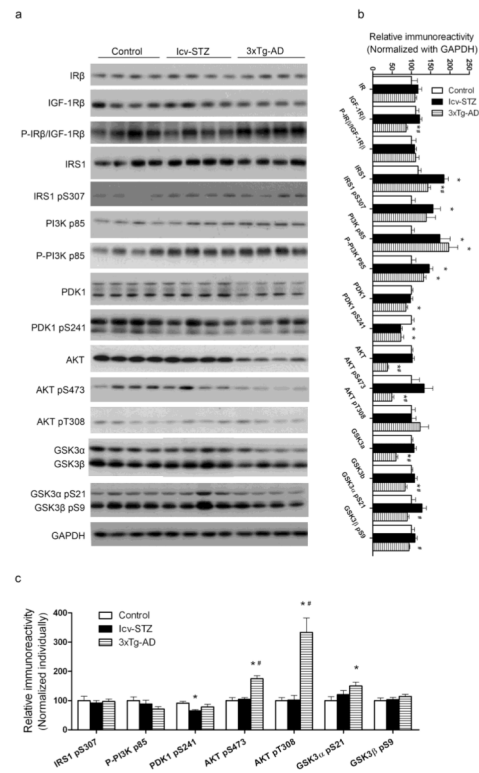
Fig. 5.
Brain insulin signaling pathway in icv-STZ and 3xTg-AD mice. (a) Hippocampi from control, icv-STZ and 3xTg-AD mice were analyzed by Western blots developed with antibodies indicated on the left of the blots. (b,c) Densitometric quantifications (mean ± SEM) of the blots after being normalized with the GAPDH levels (b) or with the levels of the corresponding total protein (c). *, $p < 0.05$ vs. control mice. #, $p < 0.05$ vs. icv-STZ mice
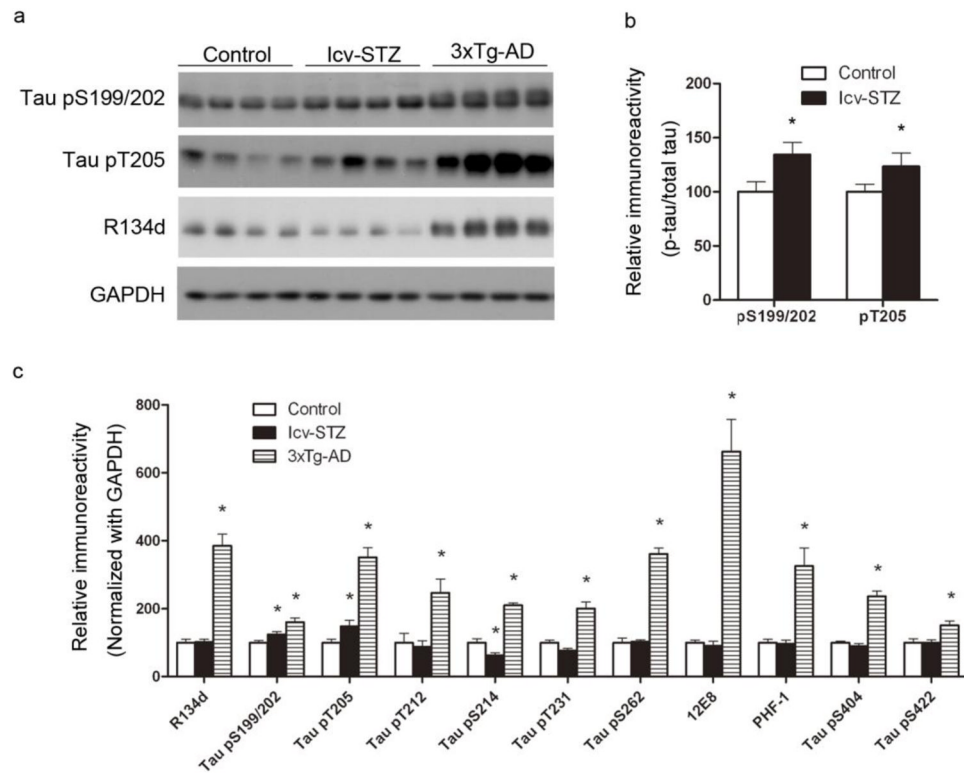
Fig. 6.
Level and phosphorylation of tau in icv-STZ mice and 3xTg-AD mice. (a) Hippocampi from control, icv-STZ and 3xTg-AD mice were analyzed by Western blots developed with antibody R134d against total tau and several phosphorylation-dependent and site-specific tau antibodies, as indicated on the left of the blots. (b,c) Densitometric quantifications (mean ± SEM) of the blots after being normalized with the total tau level (b) or with the GAPDH levels (c). *, $p < 0.05$ vs. control mice

Table 1

Primary antibodies used in this study

Antibody	Type	Specificity	Phosphorylation sites	Reference/Source
GFAP	Mono-	GFAP		Millipore, Temecula, CA
Iba1	Poly-	Iba1		Wako Chemicals, Richmond, VA
Synaptophysin	Mono-	Synaptophysin		Millipore
PSD95	Mono-	PSD95		Cell signaling Tech., Danvers, MA
GluR1	Poly-	GluR1		Millipore
GluR2/3	Mono-	GluR2/3		Abcam, Cambridge, MA, USA
NR1	Poly-	NR1		Thermo Scientific, Waltham, MA
IRβ	Poly-	IRβ		Cell signaling Tech.
IGF-1Rβ	Poly-	IGF-1Rβ		Cell signaling Tech.
P-IRβ/IGF-1Rβ	Mono-	P-IRβ/IGF-1Rβ	Tyr1135/1136 (IGF-1Rβ), Tyr1150/1151 (IRβ)	Cell signaling Tech.
IRS1	Poly-	IRS1		Cell signaling Tech.
IRS1 pS307	Poly-	P-IRS1	Ser307	Cell Signaling Tech.
PI3K p85	Poly-	PI3K (85kDa)		Cell Signaling Tech.
P-PI3K p85	Poly-	P-PI3K (85kDa)	Tyr458/Tyr199	Cell Signaling Tech.
PDK1	Poly-	PDK1		Cell Signaling Tech.
PDK1 pS241	Poly-	P-PDK1	Ser241	Cell Signaling Tech.
AKT	Poly-	AKT		Cell Signaling Tech.
AKT pS473	Poly-	P-AKT	Ser473	Cell Signaling Tech.
AKT pT308	Poly-	P-AKT	Thr308	Cell Signaling Tech.
GSK-3α/β pS21/9	Poly-	P-GSK-3β	Ser21/9	Cell Signaling Tech.
GSK-3α/β	Poly-	GSK-3β		Cell Signaling Tech.
R134d	Poly-	Tau		[59]
pS199/202	Poly-	P-tau	Ser199/2002	Invitrogen, Grand Island, NY
pT205	Poly-	P-tau	Thr205	Invitrogen
pT212	Poly-	P-tau	Thr212	Invitrogen
pS214	Poly-	P-tau	Ser214	Invitrogen
pT231	Poly-	P-tau	Thr231	Invitrogen
pS262	Poly-	P-tau	Ser262	Invitrogen
12E8	mono-	P-tau	Ser262/356	Dr. D. Schenk
PHF-1	mono-	P-tau	Ser396/404	Dr. P. Davies
pS404	Poly-	P-tau	Ser404	Invitrogen
pS422 (R145)	Poly-	P-tau	Ser422	[60]
Anti-GAPDH	Poly-	GAPDH		Santa Cruz Biotechnology